Inorg. Chem. **2007**, *46*, 3632–3644

Wide Compositional and Structural Diversity in the System Tl/Bi/P/Q (Q = S, Se) and Observation of Vicinal P–Tl *J* Coupling in the Solid State

Matthew A. Gave,[†] Christos D. Malliakas,[†] David P. Weliky,[†] and Mercouri G. Kanatzidis*[,†,‡]

Department of Chemistry, Michigan State University, East Lansing, Michigan 48824, and Department of Chemistry, Northwestern University, Evanston, Illinois 60208

Received December 22, 2006

The compounds α-$TlBiP_2Se_6$ (**I**), β-$TlBiP_2Se_6$ (**II**), $TlBiP_2S_6$ (**III**), $Tl_3Bi_3(PS_4)_4$ (**IV**), $TlBiP_2S_7$ (**V**), and $Tl_3Bi(PS_4)_2$ (**VI**) were synthesized, and the structures of **I**–**V** were determined by single-crystal X-ray diffraction analysis. The structure of **I** features infinite chains. Those of compounds **II**, **III**, and **V** are layered. The structure of **IV** features a three-dimensional framework. $Tl_4Bi_2(PS_4)_2(P_2S_6)$ (VII) was also prepared for comparison to the title compounds. The band gaps of each compound are 1.23, 1.27, 1.81, 1.88, 2.06, 1.98, and 1.97 eV for **I**–**VII**, respectively. Compounds **I**, **III**, **IV**, and **VI** melt congruently at 544, 595, 495, and 563 °C, respectively, and compounds **II**, **V**, and **VII** melt incongruently at 544, 509, and 600 °C, respectively. Solid-state ^{31}P NMR spectroscopy of the reported compounds demonstrates chemical shifts and chemical shift anisotropies in line with related chalcophosphate materials. Evidence for two-bond P–Tl *J* coupling was observed in ^{31}P NMR spectra (J = 481–1781 Hz), and to the best of our knowledge, this is the first example of two-bond P–Tl *J* coupling and the first example of P–Tl coupling in the solid state. It was possible to assign chemical shifts of inequivalent ^{31}P atoms from the same $[P_xQ_y]^{z-}$ anion type based on different modes of metal ion coordination to the chalcogen. These assignments provide information about the vicinal metal ion contribution to the ^{31}P chemical shift.

Introduction

Bismuth chalcogenide compounds have a great deal of structural diversity in part because of the flexibility of the coordination environment of Bi and the so-called inert lone-pair effect.[1] In addition to the common octahedral coordination of Bi, examples of trigonal-pyramidal,[2] square-pyramidal,[3] and capped trigonal-prismatic[4] coordination have been observed.[5] The bismuth chalcogenide building blocks can form various modules that are subsequently assembled into more complex crystalline arrangements. Examples of such assemblies can be seen in various homologous series,[6] as well as in the large class of minerals known as sulfosalts.[7] The chalcophosphate anions are a special class of chalcogenides with a broad reactivity and structural characteristics with the general formula of $[P_xQ_y]^{z-}$ (Q = S, Se). They can be stabilized as alkali-metal salts[8,9] or as coordinating ligands to a variety of metal centers.[10,11] Bi can bind to various

* To whom correspondence should be addressed. E-mail: m-kanatzidis@northwestern.edu.
† Michigan State University.
‡ Northwestern University.

(1) (a) Kanatzidis, M. G. *Chem. Mater.* **1990**, *2*, 353−363. (b) Kanatzidis, M. G.; Park, Y. *J. Am. Chem. Soc.* **1989**, *111*, 3767−3769. (c) Kanatzidis, M. G.; Park, Y. *Chem. Mater.* **1990**, *2*, 99−101. (d) Park, Y.; Kanatzidis, M. G. *Angew. Chem., Int. Ed. Engl.* **1990**, *29*, 914−915. (e) McCarthy, T. J.; Kanatzidis, M. G. *Inorg. Chem.* **1995**, *34*, 1257−1267. (f) Chondroudis, K.; Kanatzidis, M. G. *J. Solid State Chem.* **1998**, *138*, 321−328. (g) Iordanidis, L.; Bilc, D.; Mahanti, S. D.; Kanatzidis, M. G. *J. Am. Chem. Soc.* **2003**, *125*, 13741−13752.
(2) McCarthy, T. J.; Ngeyi, S.-P.; Liao, J.-H.; DeGroot, D. C.; Hogan, T.; Kannewurf, C. R.; Kanatzidis, M. G. *Chem. Mater.* **1993**, *5*, 331−340.
(3) Iordanidis, L.; Brazis, P. W.; Kyratsi, T.; Ireland, J.; Lane, M.; Kannewurf, C. R.; Chen, W.; Dyck, J. S.; Uher, C.; Ghelani, N. A.; Hogan, T.; Kanatzidis, M. G. *Chem. Mater.* **2001**, *13*, 622−633.
(4) Iordanidis, L.; Schindler, J. L.; Kannewurf, C. R.; Kanatzidis, M. G. *J. Solid State Chem.* **1999**, *143*, 151−162.
(5) (a) Kohatsu, I.; Wuensch, B. J. *Acta Crystallogr.* **1976**, *B32*, 2401−2409. (b) Cook, R.; Schafer, H. *Rev. Chim. Miner.* **1982**, *19*, 19−27. (c) Wiegers, G. A.; Meetsma, A.; Vansmaalen, S.; Haange, R. J.; Wulff, J.; Zeinstra, T.; Deboer, J. L.; Kuypers, S.; Vantendeloo, G.; Vanlanduyt, J.; Amelinckx, S.; Meerschaut, A.; Rabu, P.; Rouxel, J. *Solid State Commun.* **1989**, *70*, 409−413.
(6) (a) Mrotzek, A.; Kanatzidis, M. G. *Acc. Chem. Res.* **2003**, *36*, 111−119. (b) Kanatzidis, M. G. *Acc. Chem. Res.* **2005**, *38*, 359−368.
(7) (a) Makovicky, E. *Fortschr. Mineral.* **1981**, *59*, 137−190. (b) Makovicky, E. *Fortschr. Mineral.* **1985**, *63*, 45−89. (c) Makovicky, E. *Z. Kristallogr.* **1985**, *173*, 1−23. (d) Makovicky, E. *Neues Jahrb. Mineral., Abh.* **1989**, *160*, 269−297.
(8) Chung, I.; Do, J.; Canlas, C. G.; Weliky, D. P.; Kanatzidis, M. G. *Inorg. Chem.* **2004**, *43*, 2762−2764.
(9) Knaust, J. M.; Dorhout, P. K. *J. Chem. Crystallogr.* **2006**, *36*, 217−223.
(10) (a) Kanatzidis, M. G. *Curr. Opin. Solid State Mater. Sci.* **1997**, *2*, 139−149. (b) Coste, S.; Hanko, J.; Bujoli-Doeuff, M.; Louarn, G.; Evain, M.; Brec, R.; Alonso, B.; Jobic, S.; Kanatzidis, M. G. *J. Solid State Chem.* **2003**, *175*, 133−145.

10.1021/ic062465h CCC: $37.00
Published on Web 03/31/2007

Table 1. Crystallographic Data and Experimental and Refinement Details for Compounds **I**−**V**

	α-$TlBiP_2Se_6$ (**I**)	β-$TlBiP_2Se_6$ (**II**)	$TlBiP_2S_6$ (**III**)	$Tl_3Bi_3(PS_4)_4$ (**IV**)	$TlBiP_2S_7$ (**V**)
temp, K	298	298	298	298	298
cryst syst	monoclinic	monoclinic	monoclinic	monoclinic	monoclinic
space group	$P2_1/c$	$P2_1/c$	$P2_1$	$P2_1/c$	$P2_1$
λ(Mo Kα), Å	0.071 073	0.071 073	0.071 073	0.071 073	0.071 073
a, Å	12.539(3)	12.250(2)	6.5967(12)	20.8189(7)	9.5028(17)
b, Å	7.4990(18)	7.5518(15)	7.3749(14)	13.2281(3)	12.290(2)
c, Å	12.248(3)	22.834(5)	9.7911(18)	22.2029(7)	9.0771(16)
α, deg	90	90	90	90	90
β, deg	113.731(4)	97.65(3)	91.270(3)	117.896(2)	90.561(3)
γ, deg	90	90	90	90	90
Z	4	8	2	8	4
cryst dimens, mm	0.26 × 0.10 × 0.03	0.10 × 0.08 × 0.03	0.10 × 0.04 × 0.03	0.20 × 0.08 × 0.06	0.20 × 0.08 × 0.02
D_{calcd}, g/cm^3	5.979	6.022	4.656	4.614	4.384
μ, mm^{-1}	52.879	53.261	36.921	38.764	33.374
R_{int}, %	5.3	7.0	3.1	6.8	4.4
total reflns/ indep	6233/2495	16 039/5255	3068/1367	44 454/12 396	8406/1522
final R/R_w,[a] %	4.0/9.8	4.1/7.1	2.3/5.1	4.6/9.9	1.9/4.0

[a] $R = \sum(|F_o| - |F_c|)/\sum|F_o|$. $R_w = [\sum w(|F_o| - |F_c|)^2/\sum w|F_o|^2]^{1/2}$.

chalcophosphate ligands, such as, for example, in the compounds $KBiP_2S_7$,[12] $KBiP_2S_6$,[13] and $K_3Bi(PS_4)_2$,[14] which contain the $[P_2S_7]^{4-}$, $[P_2S_6]^{4-}$, and $[PS_4]^{3-}$ anions, respectively. Each anion can be selectively formed by slightly varying the reaction conditions, and a variety of phases can therefore be rationally synthesized.[15] In addition, chalcophosphate compounds generally are semiconductors with medium-to-wide energy gaps and can exhibit fascinating physical properties including pronounced photoconductivity and photorefractive properties,[16] pyroelectric and piezoelectric coefficients, and interesting electrooptic and nonlinear properties.[17] Nevertheless, they are relatively little investigated compounds.

Tl is often thought of as a pseudo alkali metal because of its monovalency and an ionic radius similar to that of K; however, with a lower electronegativity, the substitution of the former is expected to yield products that are less ionic in nature and, therefore, likely to feature stronger covalent bonding to the anionic framework. The effect of increased covalency results in a marked reduction in the size of the forbidden energy gap,[18−20] and, therefore, the study of this interaction could allow for the tuning of optical and electronic properties.

Because of the rich structural diversity of chalcophosphate phases and the possibility of optical and electronic tunability, we targeted the system Tl/Bi/P/Q (Q = S, Se) for investigation. Here we report six new thallium bismuth chalcophosphate compounds that have one-, two-, or three-dimensional structures and span a range of optical band gaps. The range of bonding modes of the chalcophosphate $[P_xQ_y]^{z-}$ ligands combined with the coordinative flexibility of both the Tl^+ and Bi^{3+} cations allows for rich structural chemistry in this system.

In previous studies, solid-state ^{31}P NMR has been shown to provide definitive structural information. Chemical shifts of selenophosphate compounds are strongly dependent on the type of anion present,[21] and $^{31}P-^{31}P$ dipolar coupling and ^{31}P chemical shift anisotropy are dependent on the type of chalcophosphate ion.[22] Although NMR spectroscopy provides information about the types of ions present in a compound, it is known that crystallographically inequivalent P atoms often have different chemical shifts even when only a single type of chalcophosphate ion is present. The present work provides evidence that different chemical shifts in compounds with the same anion do not arise from distortions within the $[P_xQ_y]^{z-}$ coordination geometry but instead are correlated with differences in the $[P_xQ_y]^{z-}$ ligand-to-metal ion coordination geometry. To our knowledge, this work also provides the first example of splittings due to P−Tl *J* coupling in the solid state and the first example of splitting from two-bond P−Tl *J* coupling.

Experimental Section

Reagents. Chemicals were used as obtained unless otherwise noted: bismuth chunks (Tellurex Inc., Traverse City, MI, 99.999%), selenium shot (Tellurex Inc., Traverse City, MI, 99.999%), phosphorus (MCB Reagents, Gibbstown, NJ, amorphous red),

(11) (a) Manriquez, V.; Galdamez, A.; Ruiz-Leon, D. *Mater. Res. Bull.* **2006**, *41*, 1337−1344. (b) Belkyal, I.; El Azhari, M.; Wu, Y. D.; Bensch, W.; Hesse, K. F.; Depmeier, W. *Solid State Sci.* **2006**, *8* (1), 59−63. (c) Gieck, C.; Tremel, W. *Chem.−Eur. J.* **2002**, *8*, 2980−2987. (d) Coste, S.; Kopnin, E.; Evain, M.; Jobic, S.; Brec, R.; Chondroudis, K.; Kanatzidis, M. G. *Solid State Sci.* **2002**, *4*, 709−716. (e) Hess, R. F.; Gordon, P. L.; Tait, C. D.; Abney, K. D.; Dorhout, P. K. *J. Am. Chem. Soc.* **2002**, *124*, 1327−1333. (f) Coste, S.; Kopnin, E.; Evain, M.; Jobic, S.; Payen, C.; Brec, R. *J. Solid State Chem.* **2001**, *162*, 195−203.

(12) McCarthy, T. J.; Kanatzidis, M. G. *Chem. Mater.* **1993**, *5*, 1061−1063.

(13) Manriquez, V.; Galdamez, A.; Leon, D. R.; Garland, M. T.; Jimenez, M. *Z. Kristallogr. Krist.* **2003**, *218*, 151−152.

(14) McCarthy, T. J.; Kanatzidis, M. G. *J. Alloys Compd.* **1996**, *236*, 70−85.

(15) Chung, I.; Karst, A. L.; Weliky, D. P.; Kanatzidis, M. G. *Inorg. Chem.* **2006**, *45*, 2785−2787.

(16) (a) Odoulov, S. G.; Shumelyuk, A. N.; Brost, G. A.; Magde, K. M. *Appl. Phys. Lett.* **1996**, *69*, 3665−3667. (b) Shumelyuk, A.; Hryhorashchuk, A.; Odoulov, S. *Phys. Rev. A* **2005**, *72*, 023819.

(17) Kroupa, J.; Tyagur, Y. I.; Grabar, A. A.; Vysochanskii, Y. M. *Ferroelectrics* **1999**, *223*, 421−428.

(18) McGuire, M. A.; Reynolds, T. K.; DiSalvo, F. J. *Chem. Mater.* **2005**, *17*, 2875−2884.

(19) Iyer, R. G.; Aitken, J. A.; Kanatzidis, M. G. *Solid State Sci.* **2004**, *6*, 451−459.

(20) Wachter, J. B.; Chrissafis, K.; Petkov, V.; Malliakas, C. D.; Bilc, D.; Kyratsi, Th.; Paraskevopoulos, K. M.; Mahanti, S. D.; Torbrügge, T.; Eckert, H.; Kanatzidis, M. G. *J. Solid State Chem.* **2007**, *180*, 420−431.

(21) Canlas, C. G.; Kanatzidis, M. G.; Weliky, D. P. *Inorg. Chem.* **2003**, *42*, 3399−3405.

(22) Schmedt auf der Günne, J.; Eckert, H. *Chem.−Eur. J.* **1998**, *9*, 1762−1767.

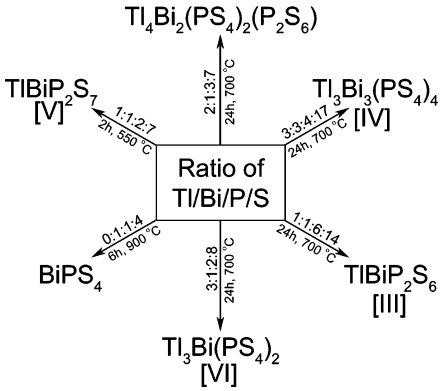

Figure 1. Schematic of the optimized reaction conditions required to produce the known Tl/Bi/P/S compounds as the dominant crystalline product. The stoichiometric ratio, soak time, and soak temperature are indicated.

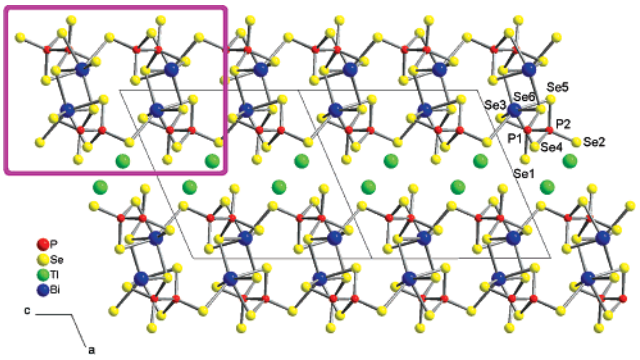

Figure 2. **I** down the (0, 1, 0) axis showing the lamellae separated by a layer of Tl^+ ions with the double-chain moiety common to **I** and **II** emphasized by the rectangular outline.

thallium metal (ABCR, Karlsruhe, Germany, 99.999%), and sublimed sulfur flowers (CCI, Vernon, CA). Se and Bi were ground in an agate mortar and pestle to ~100 mesh. P was freeze-dried with benzene.

Synthesis. (a) α-$TlBiP_2Se_6$ (I). A mixture of Tl (0.431 g, 2.1 mmol), Bi (0.4408 g, 2.1 mmol), P (0.1309 g, 4.2 mmol), and Se (0.9989 g, 12.6 mmol) was loaded into a fused-silica ampule and flame-sealed under a reduced atmosphere of $\sim 10^{-4}$ mbar. After shaking to increase homogeneity, the tube was loaded into a protective ceramic sheath and placed in a furnace. The mixture was heated to 700 °C over 24 h, held there for an additional 24 h, and then cooled back to room temperature over a period of 96 h. A homogeneous gray metallic crystalline ingot that fractured like graphite to give air-stable black plates was isolated. Energy-dispersive spectroscopic (EDS) microprobe analysis of single crystals gave an average composition of $Tl_{1.2}Bi_{1.0}P_{1.9}Se_{6.1}$.

(b) β-$TlBiP_2Se_6$ (II). A sample portion of **I** was loaded into a fused-silica ampule and flame-sealed under a reduced atmosphere of $\sim 10^{-4}$ mbar. The ampule was then heated to 400 °C over 4 h, held there for 22 days, and then qunched in air. A homogeneous gray metallic crystalline ingot that fractured like graphite to give air-stable black plates was isolated. EDS microprobe analysis gave an average composition of $Tl_{1.0}Bi_{1.0}P_{2.0}Se_{5.6}$.

(c) $TlBiP_2S_6$ (III). A mixture of Tl (0.195 g, 1.0 mmol), Bi (0.1990 g, 1.0 mmol), P (0.1768 g, 5.7 mmol), and S (13.4 mmol) was loaded into a fused-silica ampule and flame-sealed under a reduced atmosphere of $\sim 10^{-4}$ mbar. After shaking to increase homogeneity, the tube was loaded into a protective ceramic sheath and placed in a furnace. The mixture was heated to 700 °C over 12 h, held there for 24 h, and then cooled to room temperature

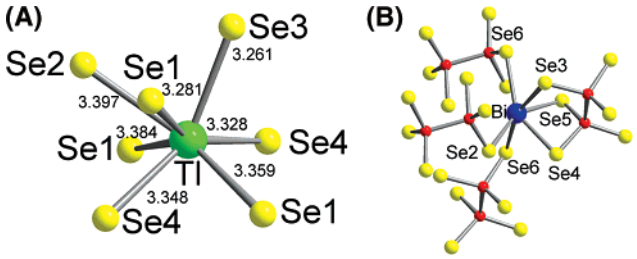

Figure 3. (A) Coordination of Tl^+ in **I** and (B) coordination of Bi^{3+} showing trischelation by one $[P_2Se_6]^{4-}$ and monodentate bonding by each of the other three $[P_2Se_6]^{4-}$ anions.

over 12 h. An ingot with a silvery surface that could be crushed to air-stable red plates was obtained. EDS microprobe analysis gave an average composition of $Tl_{1.0}Bi_{1.0}P_{2.2}S_{6.4}$.

(d) $Tl_3Bi_3(PS_4)_4$ (IV). A mixture of Tl (0.321 g, 1.6 mmol), Bi (0.3288 g, 1.6 mmol), P (0.0649 g, 2.1 mmol), and S (0.2861 g, 8.9 mmol) was loaded into a fused-silica ampule and treated as described above. The mixture was reacted with the same heating profile as that in **I**. A deep-red crystalline ingot that was composed of air-stable red plates was isolated. Microprobe analysis gave an average composition of $Tl_{1.1}Bi_{1.0}P_{1.3}S_{5.0}$.

(e) $TlBiP_2S_7$ (V). A mixture of Tl (0.2921 g, 1.4 mmol), Bi (0.2980 g, 1.4 mmol), P (0.0883 g, 2.9 mmol), and S (0.3201 g, 9.7 mmol) was loaded into a fused-silica ampule and treated as described above. The mixture was heated to 550 °C over 3 h, held there for 2 h, and then cooled to room temperature over 12 h. A silvery ingot that was composed of air-stable red plates was isolated. Microprobe analysis gave an average composition of $Tl_{1.0}Bi_{1.0}P_{1.9}S_{6.9}$.

(f) $Tl_3Bi(PS_4)_2$ (VI). A mixture of Tl (1.076 g, 5.3 mmol), Bi (0.3670 g, 1.8 mmol), P (0.1083 g, 3.5 mmol), and S (0.4504 g, 14.0 mmol) was loaded into a fused-silica ampule and treated as described above. The mixture was then allowed to react with the same heating profile as that in **I**. A silvery ingot that fractured into bright-red plates was isolated. Microprobe analysis of several crystals gave an average composition of $Tl_{3.1}Bi_{1.0}P_{1.8}S_{8.4}$.

Single crystals of **VI** with high enough quality to obtain a satisfactory refinement could not be obtained. Many crystals were screened, and all showed evidence of twinning in the form of a rotational smearing of higher angle spots perpendicular to (0, 0, 1).[23] Presumably, each crystal that was mounted was a stack of plates with a slight rotation from one plate to the next.

It was possible to index the data with a monoclinic cell with $a = 25.314(5)$ Å, $b = 6.660(1)$ Å, $c = 17.950(1)$ Å, $\beta = 110.67(3)°$, $Z = 8$, and $V = 2831.6(13)$ Å^3. A solution in the $P2_1/c$ space group was found that shows the same zigzag $[Bi(PS_4)_2]_n^{3n-}$ chains as those in $K_3Bi(PS_4)_4$.[14] The model did not converge, as was evidenced by a relatively high reliability factor (~12%), negative thermal parameters, and high residual peaks of electron density. Furthermore, the model suggested a positional disorder of the Bi^{3+} ions down the chain axis that resulted in a 50% occupation of the Bi^{3+} ions in each of two different sites. The space group $P2_1$ was also tested to verify that the 50%/50% disorder was not a result of an artificial symmetry restriction. A significant improvement in reliability statistics was not obtained.

A view of an intensity-weighted reciprocal lattice suggested that the monoclinic cell might not have been the most appropriate choice

(23) A figure of the reciprocal lattice illustrating the smearing of spots, a representation of the relationship between the two proposed unit cells, and a simulated precession photo of $Tl_3Bi(PS_4)_4$ can be found in the Supporting Information.

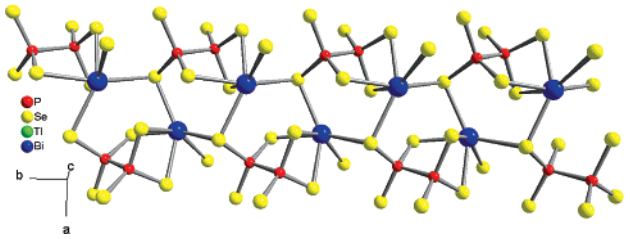

Figure 4. Assembly of the chain common to both **I** and **II** viewed down the (0, 0, 1) axis.

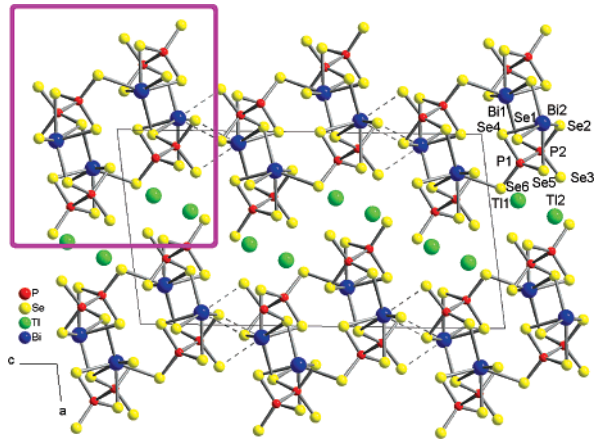

Figure 5. **II** down the (0, 1, 0) axis showing emphasis on the weak interchain interaction with a dashed line and a double-chain moiety common to **I** and **II** emphasized by a rectangular outline.

because it was possible to index a smaller orthorhombic cell that was close to the cell of the K analogue[14] with a superstructure or modulation vector to describe the remaining reflections. An orthorhombic unit cell with $a = 8.973(2)$ Å, $b = 6.653(1)$ Å, and $c = 23.676(5)$ Å was used to describe the main reflections, and the remaining reflections could be indexed using a modulation vector of ($^1/_2$, 0, $^1/_2$). This cell becomes the initial cell when doubled in the *a* and *c* crystallographic directions and transformed to the monoclinic setting. The refinement of the structure in the space group *Pnma* converged to a final *R* value of about 8.8%, but a suitable super space group could not be found that modeled the satellite reflections. The K analogue has $P2_12_12_1$ symmetry, a space group that is a minimal non-isomorphic subgroup of *Pnma*. Although a convergent model was obtained using $P2_12_12_1$, it did not result in a significant decrease in reliability statistics and again it was not possible to find a suitable corresponding super space group. The cell obtained by doubling the *a* and *c* axes removes the need for the modulation vector and is the orthorhombic translation of the above monoclinic cell, but no convergent model using this doubled cell was found.

(g) $Tl_4Bi_2(PS_4)_2(P_2S_6)$ (VII). Though the structure of **VII** was previously reported,[18] the authors made no attempt to optimize the synthesis. Crystals of **VII** were obtained from a mixture of Tl (0.874, 4.3 mmol), Bi (0.3670 g, 2.1 mmol), P (0.1990 g, 6.4 mmol), and S (0.4795 g, 15.0 mmol) loaded into a fused-silica ampule and flame-sealed under a reduced pressure of $\sim 10^{-4}$ mbar. After shaking to increase homogeneity, the tube was loaded into a protective ceramic sheath and placed in a furnace. The mixture was then allowed to react with the same heating profile as those in **I**. A homogeneous-looking silvery ingot that fractured into bright-red plates was isolated. Presumably, a minor amorphous P/S-containing byproduct is present but could not be observed. EDS microprobe analysis of several crystals gave an average composition of $Tl_{2.3}Bi_{1.0}P_{2.8}S_{11.1}$.

Table 2. Selected Bond Lengths (Å) and Angles (deg) for **I**, with Standard Uncertainties in Parentheses[a]

Bi−Se5	2.8506(14)	Se5−Bi−Se4	75.90(4)
Bi−Se4	2.8676(14)	Se5−Bi−Se3	86.42(4)
Bi−Se3	2.9148(12)	Se4−Bi−Se3	82.88(3)
Bi−Se6	3.0531(13)	Se5−Bi−Se6	80.18(4)
Bi−Se6^{i}	3.0919(13)	Se4−Bi−Se6	80.89(3)
Bi−Se2	3.1253(14)	Se3−Bi−Se6	161.03(4)
		Se5−Bi−Se6^{i}	79.78(3)
Tl−Se3	3.2615(14)	Se4−Bi−Se6^{i}	146.07(3)
Tl−Se1	3.2814(15)	Se3−Bi−Se6^{i}	72.25(3)
Tl−Se4^{v}	3.3277(14)	Se6−Bi−Se6^{i}	117.86(3)
Tl−Se4^{iv}	3.3476(14)	Se5−Bi−Se2	149.99(4)
Tl−Se1^{iv}	3.3590(13)	Se4−Bi−Se2	74.12(4)
Tl−Se1^{vi}	3.3843(14)	Se3−Bi−Se2	91.25(3)
Tl−Se2^{vii}	3.3974(14)	Se6−Bi−Se2	93.68(3)
Tl−Se2^{viii}	3.6999(15)	Se6^{i}−Bi−Se2	127.80(4)
Se1−P1	2.155(3)	Se1−P1−Se6^{vii}	113.62(12)
Se2−P2	2.160(3)	Se1−P1−Se3	114.65(14)
Se3−P1	2.220(3)	Se6^{vii}−P1−Se3	111.94(13)
Se4−P2^{ii}	2.197(3)	Se2−P2−Se4^{v}	116.69(14)
Se5−P2^{ii}	2.222(3)	Se2−P2−Se5^{v}	116.07(14)
Se6−P1^{iii}	2.203(3)	Se4^{v}−P2−Se5^{v}	105.46(12)
P1−P2^{ii}	2.228(4)	Se2−P2−P1^{v}	108.57(13)
		Se1−P1−P2^{ii}	108.30(15)
		Se6^{vii}−P1−P2^{ii}	102.37(15)
		Se3−P1−P2^{ii}	104.71(13)
		Se4^{v}−P2−P1^{v}	103.47(15)
		Se5^{v}−P2−P1^{v}	105.32(14)

[a] (i) $-x$, $0.5 + y$, $0.5 - z$; (ii) x, $0.5 - y$, $-0.5 + z$; (iii) x, $-1 + y$, z; (iv) $1 - x$, $1 - y$, $1 - z$; (v) x, $0.5 - y$, $0.5 + z$; (vi) x, $1.5 - y$, $0.5 + z$; (vii) x, $1 + y$, z; (viii) $1 - x$, $0.5 + y$, $1.5 - z$; (ix) x, $1.5 - y$, $-0.5 + z$; (x) $1 - x$, $-0.5 + y$, $1.5 - z$; (xi) $-x$, $-0.5 + y$, $0.5 - z$.

Powder X-ray Diffraction. All samples were assessed for phase purity using powder X-ray diffraction. Powder patterns were obtained using an Inel CPS 120 powder X-ray diffractometer with monochromatized Cu Kα radiation ($\lambda = 1.540\,598$ Å) operating at 40 kV and 20 mA, equipped with a position-sensitive detector with a 2θ range of 0−120°, and calibrated with LaB_6.

Single-Crystal X-ray Diffraction. Intensity data for single crystals of **I**−**VI** were collected on a Bruker SMART platform CCD diffractometer using Mo Kα radiation operating at 40 kV and 40 mA. A full sphere of data was collected, and individual frames were acquired with a 10-s exposure time and a 0.3° ω rotation. The *SMART* software was used for data collection, and *SAINT* software was used for data extraction and reduction. An analytical absorption correction to the data was performed, and direct methods were used to solve and refine the structures with the *SHELXTL*[24] software package.

Intensity data for several crystals of **VI** were also collected on a STOE IPDS II diffractometer with Mo Kα radiation operating at 50 kV and 40 mA on a 34-cm image plate. Individual frames were collected with a 60-s exposure time and a 0.5° ω rotation. The *X-SHAPE* and *X-RED* software packages were used for data extraction and reduction and for application of an analytical absorption correction. The *SHELXTL* and *JANA2000*[25] software packages were used to solve and refine the structure. The parameters for data collection and the details of the structural refinement are given in Table 1.

Energy-Dispersive Spectroscopy. A JEOL JSM-35C scanning electron microscope equipped with a Tracor Northern EDS detector

(24) *SHELXTL* version 5; Bruker Analytical X-ray Instruments Inc.: Madison, WI, 1998.
(25) Petricek, V.; Dusek, M.; Palatinus, L. **2000**. *Jana2000. The crystallographic computing system*; Institute of Physics: Praha, Czech Republic, 2000.

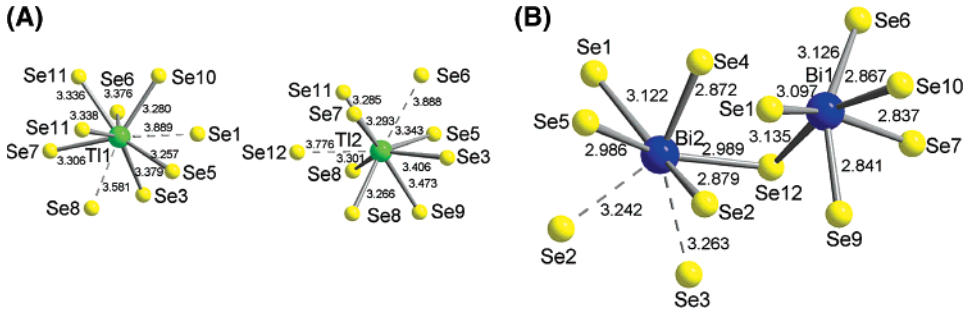

Figure 6. (A) Coordination of Tl^{+} in **II** and (B) coordination of Bi^{3+} showing the weak interchain Bi−Se interaction with a dashed line.

was used for quantitative microprobe analysis. Data were collected using an accelerating voltage of 25 kV and a collection time of 60 s, and results were averaged over several sample areas.

Differential Thermal Analysis. Differential thermal analyses were performed with a Shimadzu DTA-50 thermal analyzer. A ground sample weighing ~25 mg was sealed in a quartz ampule under reduced pressure. An equivalent mass of alumina was sealed in an identical ampule to serve as a reference. The samples were heated to 850 °C at a rate of 10 °C/min, cooled to 150 °C at a rate of 10 °C/min, reheated to 850 °C at a rate of 10 °C/min, and then cooled to room temperature at a rate of 10 °C/min.

UV/vis Spectroscopy. Optical band gaps were determined using the Kubelka−Munk theory[26] on data collected by diffuse-reflectance UV/vis spectroscopy on finely ground samples at room temperature. A background was collected before each scan using $BaSO_4$. A spectrum was collected for the region of 200−2500 nm with a Shimadzu UV-3101 PC double-beam, double-monochromator spectrophotometer.

NMR Spectroscopy. Room-temperature solid-state NMR spectra of **I**−**VII** were collected on a 9.4 T spectrometer (Varian Infinity Plus) using a double-resonance magic-angle-spinning (MAS) probe. Samples were spun at frequencies ranging from 5 to 15 kHz in zirconia rotors of 4-mm-outer diameter and with a ~50-μL sample volume. Bloch decay spectra were taken with a 4-μs 90° pulse (calibrated using 85% H_3PO_4) and with relaxation delays ranging from 10 to 5000 s. Each spectrum was processed with ≤100-Hz line broadening and up to a 10th-order polynomial baseline correction. The spectra were referenced to 85% H_3PO_4 at 0 ppm.

Quantitative spectra were collected by ensuring that the pulse delay between scans was at least 2−5 times T_1. All of the compounds except **I** and **III** had T_1 relaxation times in the range of 1500−1750 s, which is typical for the chalcophosphate compounds previously studied.[27]

Room-temperature solid-state NMR spectra of **VI** and **VII** were also collected on a Bruker DSX300 NMR spectrometer using a double-resonance MAS probe with zirconia rotors of 4-mm-outer diameter. Bloch decay spectra were collected with a 4.5-μs 90° pulse and a relaxation delay of 2500 s.

Results and Discussion

Synthetic Reactions. It was possible to form **I** by a direct combination of the elements. The compound **II**, however, was not formed directly from the melt but was instead formed after the α phase was annealed for an extended period of time (~22 days) below the melting point. Presumably then, the α compound is the kinetically stable one, whereas the β phase is thermodynamically stable. The rotation of the chain (vide infra) that accounts for the difference between the two compounds likely has a high energy of activation, and a short (i.e., several hours to several days) annealing time is insufficient to affect such a conversion. Though the α-$MBiP_2Se_6$ (M = K, Tl) phases are isomorphous, it is interesting to note that β-$TlBiP_2Se_6$ and β-$KBiP_2Se_6$[28] are different structure types, with the latter being formed after a glass formed by rapid quenching was annealed. As in the case of the K analogue, it was possible to form a glass by quenching a stoichiometric melt of Tl/Bi/2P/6Se, but after the glass was annealed, the α phase was again isolated. A Tl^{+}-containing compound that is isomorphous to β-$KBiP_2Se_6$[32] was not found.

Compounds **III** and **IV** have a 1:1 ratio of Tl to Bi. By slight variation of the reaction conditions, it was possible to prepare each as the dominant crystalline phase. On the basis of the experimental information we have gathered thus far, we can produce a schematic reactivity table that places these compounds in a greater context, as shown in Figure 1. It was initially a challenge to reproduce **V** because **IV** often formed. **IV** was originally discovered with reaction conditions identical with those used for **I** but with S instead of Se. The intended **III** stoichiometry was not produced by this reaction, but rather **IV** was produced as the dominant crystalline product. Although its presence could not be confirmed with powder X-ray diffraction, **IV** must have been accompanied by a glassy phase composed of the extra 2 equiv of both P and S. Upon further investigation, it was determined that the additional P is not necessary to produce compound **IV** in pure form but that some additional S is essential. The optimized reaction conditions for producing compound **IV** were determined to be 3Tl/3Bi/4P/17S, that is, an extra 1 equiv of S. It is possible that the extra 1 equiv of S in the form of S_x^{2-} chains reduced the acidity of the melt, wherein compound **IV** could be formed. The metal-to-chalcogenide ratio is extremely important in the melt, and changes of as little as 0.2 stoichiometric equiv were observed to have the marked effect of producing a completely different crystalline compound.[29]

(26) (a) Wendlandt, W. W.; Hecht, H. G. *Reflectance Spectroscopy*; Interscience Publishers: New York, 1966. (b) Kotum, G. *Reflectance Spectroscopy*; Springer-Verlag: New York, 1969. (c) Tandon, S. P.; Gupta, J. P. *Phys. Status Solidi* **1970**, *38*, 363−367.
(27) Canlas, C. G.; Mathukumaran, R. B.; Kanatzidis, M. G.; Weliky, D. P. *Solid State Nucl. Magn. Reson.* **2003**, *24*, 110−122.
(28) Breshears, J. D.; Kanatzidis, M. G. *J. Am. Chem. Soc.* **2000**, *122*, 7839−7840.
(29) Kanatzidis, M. G.; Sutorik, A. C. *Prog. Inorg. Chem.* **1995**, *43*, 151−265.

Table 3. Selected Bond Lengths (Å) and Angles (deg) for **II**, with Standard Uncertainties in Parentheses[a]

Bi1−Se7	2.8374(14)	Se7−Bi1−Se9	76.47(5)
Bi1−Se9	2.8406(16)	Se7−Bi1−Se10	83.56(4)
Bi1−Se10	2.8671(13)	Se9−Bi1−Se10	86.70(4)
Bi1−Se1	3.0974(14)	Se7−Bi1−Se1	147.24(3)
Bi1−Se6	3.1259(16)	Se9−Bi1−Se1	79.83(4)
Bi1−Se12	3.1352(14)	Se10−Bi1−Se1	72.73(4)
Bi2−Se4	2.8717(16)	Se7−Bi1−Se6	72.68(4)
Bi2−Se2	2.8786(13)	Se9−Bi1−Se6	149.08(4)
Bi2−Se5	2.9858(14)	Se10−Bi1−Se6	91.84(4)
Bi2−Se12	2.9885(14)	Se1−Bi1−Se6	129.04(4)
Bi2−Se1^{ii}	3.1226(13)	Se7−Bi1−Se12	79.90(4)
Bi2−Se2^{iii}	3.2419(16)	Se9−Bi1−Se12	80.29(4)
Bi2−Se3^{iv}	3.2627(18)	Se10−Bi1−Se12	160.93(4)
		Se1−Bi1−Se12	117.98(4)
Tl1−Se5	3.2565(15)	Se6−Bi1−Se12	92.23(4)
Tl1−Se10^{i}	3.2802(17)	Se4−Bi2−Se2	85.74(4)
Tl1−Se7^{v}	3.3065(13)	Se4−Bi2−Se5	73.89(4)
Tl1−Se11^{vi}	3.3356(17)	Se2−Bi2−Se5	80.19(4)
Tl1−Se11^{vii}	3.3377(14)	Se4−Bi2−Se12	80.26(4)
Tl1−Se6^{vi}	3.3764(14)	Se2−Bi2−Se12	75.12(4)
Tl1−Se3^{v}	3.3792(17)	Se5−Bi2−Se12	145.30(3)
Tl1−Se8^{iii}	3.5813(17)	Se4−Bi2−Se1^{ii}	78.94(4)
Tl2−Se8	3.2658(17)	Se2−Bi2−Se1^{ii}	155.90(4)
Tl2−Se11	3.2846(17)	Se5−Bi2−Se1^{ii}	77.76(4)
Tl2−Se7	3.2928(15)	Se12−Bi2−Se1^{ii}	119.71(4)
Tl2−Se8^{iv}	3.3008(14)	Se4−Bi2−Se2^{iii}	139.90(4)
Tl2−Se5^{viii}	3.3434(14)	Se2−Bi2−Se2^{iii}	89.19(3)
Tl2−Se3	3.4056(14)	Se5−Bi2−Se2^{iii}	66.05(4)
Tl2−Se9^{iv}	3.4733(18)	Se12−Bi2−Se2^{iii}	136.31(4)
Tl2−Se12	3.7761(15)	Se1^{ii}−Bi2−Se2^{iii}	90.66(4)
Tl2−Se6^{ix}	3.8876(18)	Se4−Bi2−Se3^{iv}	141.72(4)
		Se2−Bi2−Se3^{iv}	65.25(4)
Se1−P2^{vii}	2.194(3)	Se5−Bi2−Se3^{iv}	121.30(4)
Se2−P2^{vii}	2.219(4)	Se12−Bi2−Se3^{iv}	68.89(4)
Se3−P2	2.165(4)	Se1^{ii}−Bi2−Se3^{iv}	135.98(3)
Se4−P1	2.220(3)	Se2^{iii}−Bi2−Se3^{iv}	67.51(4)
Se5−P1	2.172(4)		
Se6−P1^{i}	2.159(4)	Se6^{i}−P1−Se5	118.15(15)
Se7−P4^{xii}	2.205(4)	Se6^{i}−P1−Se4	115.33(18)
Se8−P4	2.127(4)	Se5−P1−Se4	106.61(13)
Se9−P4^{xii}	2.220(3)	Se6^{i}−P1−P2^{vii}	107.38(14)
Se10−P3^{x}	2.213(4)	Se5−P1−P2^{vii}	103.14(17)
Se11−P3	2.156(3)	Se4−P1−P2^{vii}	104.76(15)
Se12−P3	2.204(3)	Se3−P2−Se1^{viii}	115.13(13)
		Se3−P2−Se2^{viii}	111.08(17)
P1−P2^{vii}	2.230(4)	Se1^{viii}−P2−Se2^{viii}	113.52(14)
P4−P3^{xii}	2.246(4)	Se3−P2−P1^{viii}	108.35(16)
		Se1^{viii}−P2−P1^{viii}	104.11(17)
		Se2^{viii}−P2−P1^{viii}	103.61(13)
		Se11−P3−Se12	112.38(13)
		Se11−P3−Se10^{ii}	114.84(18)
		Se12−P3−Se10^{ii}	112.18(14)
		Se11−P3−P4^{iv}	108.44(15)
		Se12−P3−P4^{iv}	102.62(16)
		Se10^{ii}−P3−P4^{iv}	105.29(14)
		Se8−P4−Se7^{iv}	115.78(15)
		Se8−P4−Se9^{iv}	118.31(18)
		Se7^{iv}−P4−Se9^{iv}	105.16(13)
		Se8−P4−P3^{xii}	110.08(14)
		Se7^{iv}−P4−P3^{xii}	101.93(17)
		Se9^{iv}−P4−P3^{xii}	103.73(15

[a] (i) $-x, 1-y, -z$; (ii) $x, -1+y, z$; (iii) $-x, -0.5+y, 0.5-z$; (iv) $1-x, -0.5+y, 0.5-z$; (v) $-1+x, -1+y, z$; (vi) $-x, -y, -z$; (vii) $-1+x, y, z$; (viii) $1+x, y, z$; (ix) $1-x, 1-y, -z$; (x) $x, 1+y, z$; (xi) $-x, 0.5+y, 0.5-z$; (xii) $1-x, 0.5+y, 0.5-z$; (xiii) $1+x, 1+y, z$.

A stoichiometric combination of 3Tl/3Bi/4P/16S did not produce compound **IV** but gave a product that contained a significant amount of **III** along with $BiPS_4$ as a minor phase. In terms of a 1:1 Tl/Bi ratio, this results in a deficiency of both P and S relative to the stoichiometry of the dominant crystalline compound, suggesting that the S was consumed by oxidation of the metals before P could be fully oxidized to the 5+ state. To produce compound **III** as the dominant crystalline product, it was therefore necessary to employ a flux with limited acidity to stabilize the $[P_2S_6]^{4-}$ unit.[30]

Compound **V** was formed from a nearly stoichiometric mixture of the elements but with a heating profile that was both lower in temperature and shorter in time than any of the other reactions. When slowly cooled, a mixture of Tl/Bi/2P/7S produced mainly compound **IV** but also some $BiPS_4$. Presumably, compound **V** is more kinetically stable, and a more rapid cooling rate is necessary to avoid the more thermodynamically stable compounds.

It was also possible to prepare **VII**[18] in pure form by adding an additional 1 equiv of P (i.e., 2Tl/Bi/3P/7S). The overoxidation of P to 5+ was prevented by the extra P, and it was possible to stabilize both the P^{4+} and P^{5+} species in the compound.[31]

Structure Description. (a) Compounds I and II. I is isomorphous with α-KMP_2Se_6[32] (M = Sb, Bi; Figure 2). The structure is built up of $[MP_2Se_6]^-$ layers that are separated by Tl^+ ions with a mean Tl−Se distance of 3.34 Å. Comparatively, the K^+ analogue has K−Se bond distances averaging 3.36 Å. Each Tl^+ cation is seven-coordinate with a distorted monocapped-octahedral geometry (Figure 3A), and each Bi has is six-coordinate with four different $[PS_4]^{3-}$ units (Figure 3B). One of the $[P_2Se_6]^{4-}$ anions is trischelated to Bi^{3+} (Se3, Se4, and Se5) with Bi−Se bonds ranging from 2.8506(14) to 3.1253(14) Å in length. Neighboring BiS_6 are connected to form a chain down (0, 1, 0) by bridging Bi−Se6 bonds at a distance of 3.1253(14) Å. Finally, a double chain is assembled through the Bi−Se2 bond where Se2 is on a $[P_2Se_6]^{4-}$ ion in a neighboring chain along the (0, 0, 1) axis. Neighboring double chains are assembled by the same Bi−Se2 bond. The layer assembled from the double chains is separated from an identical layer by Tl^+ ions. The P−P bond distance in the $[P_2Se_6]^{4-}$ anion is 2.228(4) Å, and the P−Se bond distances range from 2.155(3) to 2.222(3) Å. There is one Se atom on the $[P_2Se_6]^{4-}$ anion that is terminal and interacts only with Tl^+ ions. Table 2 contains selected bond lengths and angles for compound **I**.

The compound **II** crystallizes in the monoclinic space group $P2_1/c$. The structure is built up from the same chains as those described in α-$KBiP_2Se_6$ and α-$TlBiP_2Se_6$. The difference between compounds **I** and **II** is that, in the latter, the layer is broken apart by a rotation about the (0, 1, 0) axis of $[BiP_2Se_6]_4^{4-}$ double chains such that one-dimensionality is preserved (Figures 4 and 5). There are two such chains per unit cell, with one centered at the origin and the other centered along the *c* axis. Each chain is separated along

(30) A reaction with the stoichiometric ratio of Tl/Bi/6P/14S was subsequently found to produce compound **III** as the sole crystalline product. Attempts to remove the glassy impurities by washing with ethylenediamine, methanol, and ether resulted in a product that was amorphous by powder X-ray diffraction, suggesting that compound **III** decomposes under such conditions.

(31) Gave, M. A.; Bilc, D.; Mahanti, S. D.; Breshears, J. D.; Kanatzidis, M. G. *Inorg. Chem.* **2005**, *44*, 5293−5303.

(32) McCarthy, T. J.; Kanatzidis, M. G. *J. Chem. Soc., Chem. Commun.* **1994**, 1089−1090.

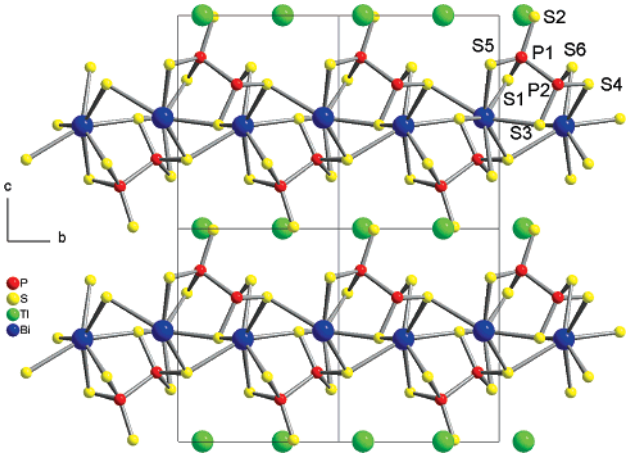

Figure 7. Structure of **III** viewed down the (1, 0, 0) axis showing the lamellar stacking motif.

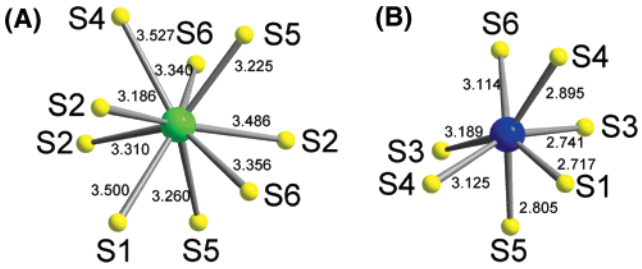

Figure 8. (A) Tl^{+} coordination environment and (B) coordination environment of Bi^{3+} in **III**.

the (1, 0, 0) direction by Tl^{+} ions. Tl1 forms a distorted bicapped octahedron. Seven of the Tl−Se distances are relatively short, with an average distance of 3.40 Å. The remaining interaction between Tl1 and Se8 is weak with a bond length of 3.5813(17) Å. Tl2 is also a distorted bicapped octahedron, again with seven short and one longer Tl−Se interactions. The average length of the shorter bonds is 3.34 Å, and the longer Tl2−Se12 interaction is 3.7761(15) Å (Figure 6A).

Each Bi^{3+} center is trischelated by Se atoms with an average Bi−Se bond length of 2.88 Å (Figure 6B). Two chains are then connected together to form a double chain with a Bi1−Se6 bond length of 3.1259(16) Å, and the chains interact weakly with neighboring double chains with a Bi2−Se2 bond length of 3.2419(16) Å and a Bi2−Se3 bond length of 3.2627(18) Å (Figure 6B). Table 3 contains selected bond lengths and angles for compound **II**.

(b) Compound III. III crystallizes in the monoclinic space group $P2_1$. The structure is closely related to that of K(RE)-P_2Se_6 (RE = Y, Gd)[33] and isomorphous to β-KMP_2Se_6 (M = Sb, Bi)[28] and $KBiP_2S_6$.[13] The structure is composed of $[Bi(P_2S_6)]^{-}$ layers separated by Tl^{+} cations (Figure 7). The Tl^{+} ions are spherically coordinated by nine S atoms with an average Tl−S interaction of 3.35 Å (Figure 8A). The Bi^{3+} atoms are trischelated by a $[P_2S_6]^{4-}$ anion with Bi−Se distances ranging from 2.717(3) to 2.805(3) Å. A second $[P_2S_6]^{4-}$ anion is chelated to the Bi^{3+} cation with Bi−S bond distances of 2.741(3) and 3.114(3) Å. Two other $[P_2S_6]^{4-}$ anions are chelated to the Bi^{3+} cation with a Bi−S distance of 3.125(3) Å (Figure 8B). The P−P distance is 2.221(4) Å. Table 4 contains selected bond lengths and angles for compound **III**. The difference between the Se-containing compounds (i.e., **I** and **II**) and compound **III** is that, in the former, the Bi^{3+} ions undulate in a direction perpendicular to the chain between two different positions down the length of the chain, so that when the chains assemble, they form a slab that has a thickness of two $[P_2Se_6]^{4-}$-capped Bi^{3+} ions. In compound **III**, the Bi^{3+} ions do not undulate, and therefore the resulting slab is only one Bi^{3+} coordination environment thick.

Table 4. Selected Bond Lengths (Å) and Angles (deg) for **III**, with Standard Uncertainties in Parentheses[a]

Tl−S2^{i}	3.186(3)	S1−Bi−S3	84.78(10)
Tl−S5	3.225(3)	S1−Bi−S5^{vii}	72.88(9)
Tl−S5^{ii}	3.261(3)	S3−Bi−S5^{vii}	81.06(9)
Tl−S2	3.310(3)	S1−Bi−S4^{v}	81.34(9)
Tl−S6^{iii}	3.340(3)	S3−Bi−S4^{v}	76.90(9)
Tl−S6^{iv}	3.356(3)	S5^{vii}−Bi−S4^{v}	147.35(9)
Tl−S2^{v}	3.486(3)	S1−Bi−S6	145.26(9)
Tl−S1^{vi}	3.499(3)	S3−Bi−S6	67.85(8)
Tl−S4	3.527(3)	S5^{vii}−Bi−S6	120.66(8)
		S4^{v}−Bi−S6	72.17(8)
Bi−S1	2.717(3)	S1−Bi−S4^{vii}	81.08(9)
Bi−S3	2.741(3)	S3−Bi−S4^{vii}	157.26(8)
Bi−S5^{vii}	2.805(3)	S5^{vii}−Bi−S4^{vii}	77.82(8)
Bi−S4^{v}	2.895(3)	S4^{v}−Bi−S4^{vii}	118.04(6)
Bi−S6	3.114(3)	S6−Bi−S4^{vii}	131.19(8)
Bi−S4^{vii}	3.125(3)		
		S2^{v}−P1−S5^{ii}	116.26(19)
P1−S2^{v}	1.967(4)	S2^{v}−P1−S1^{x}	118.5(2)
P1−S5^{ii}	2.038(4)	S5^{ii}−P1−S1^{x}	106.4(2)
P1−S1^{x}	2.060(4)	S6^{iv}−P2−S4^{v}	114.09(18)
P2−S6^{iv}	2.003(4)	S6^{iv}−P2−S3^{x}	112.0(2)
P2−S4^{v}	2.035(4)	S4^{v}−P2−S3^{x}	112.21(19)
P2−S3^{x}	2.062(4)		
		S2^{v}−P1−P2	109.6(2)
P1−P2	2.221(4)	S5^{ii}−P1−P2	101.59(18)
		S1^{x}−P1−P2	102.35(18)
		S6^{iv}−P2−P1	108.37(17)
		S4^{v}−P2−P1	105.52(19)
		S3^{x}−P2−P1	103.80(16)

[a] (i) $1-x$, $0.5+y$, $-z$; (ii) $-x$, $-0.5+y$, $-z$; (iii) $-1-x$, $-0.5+y$, $-z$; (iv) $1+x$, y, z; (v) $-x$, $0.5+y$, $-z$; (vi) $-x$, $-0.5+y$, $-1-z$; (vii) $-1+x$, y, $-1+z$; (viii) $-1+x$, y, z; (ix) $-1-x$, $0.5+y$, $-1-z$; (x) $-1-x$, $-0.5+y$, $-1-z$; (xi) $-x$, $0.5+y$, $-1-z$; (xii) $1-x$, $-0.5+y$, $-z$; (xiii) x, $-1+y$, z; (xiv) $-1-x$, $0.5+y$, $-z$; (xv) $1+x$, y, $1+z$.

(c) Compound IV. IV crystallizes in the monoclinic space group $P2_1/c$.[34] The three-dimensional structure of the compound can be seen as an assembly of $[Bi_3(PS_4)_4]^{3-}$ slabs stacked along the *b* axis (Figure 9A). The slabs are interconnected with Bi−S bonds and form channels in each direction that are occupied by Tl atoms (Figure 9B).

(33) Chen, J. H.; Dorhout, P. K.; Ostenson, J. E. *Inorg. Chem.* **1996**, *35*, 5627−5633.

(34) Crystal twinning in a merohedral fashion was a major difficulty in solving and refining the structure. Data sets on several crystals were collected but could not be successfully refined, as large residual electron densities remained. Careful examination of the reciprocal lattice revealed a second twin domain rotated 180° along the *a* axis. When the corresponding twin law of

$$\begin{bmatrix} a' \\ b' \\ c' \end{bmatrix} = \begin{bmatrix} 1 & 0 & 0 \\ 0 & -1 & 0 \\ -1 & 0 & -1 \end{bmatrix} \begin{bmatrix} a \\ b \\ c \end{bmatrix}$$

was applied, the *R* value dropped from 28% to 5%. This led to small residuals in the electron density map and with a twin fraction of 43.2-(1)%.

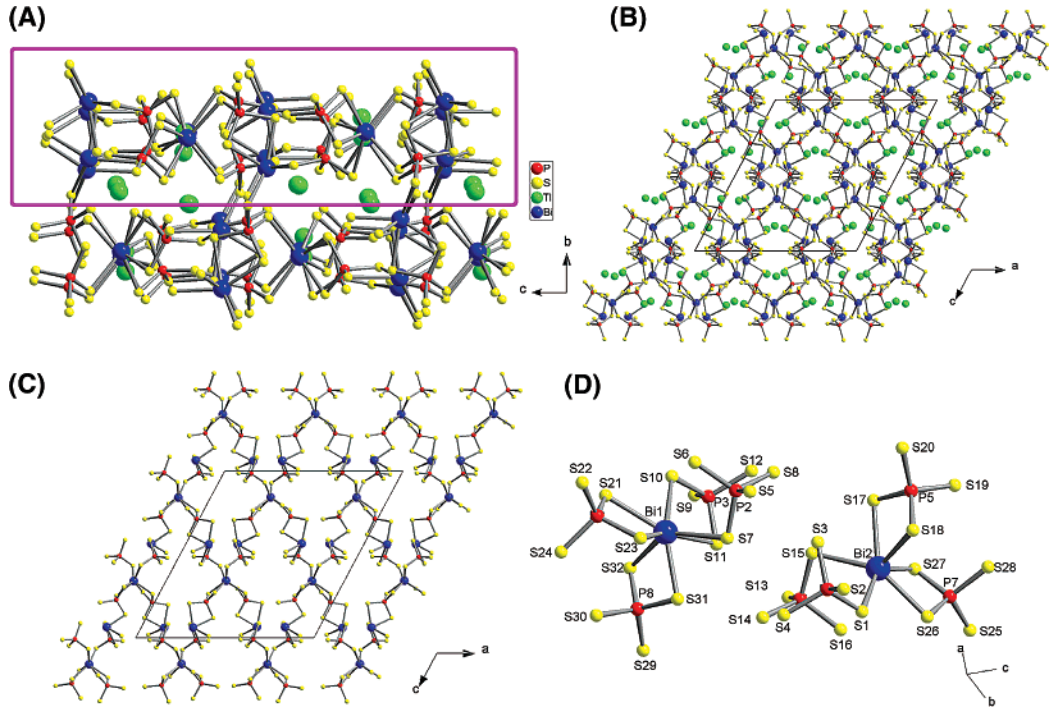

Figure 9. (A) **IV** viewed down the (1, 0, 0) axis showing the stacking of **IV** along the *b* axis with a slab emphasized by a rectangular outline, (B) view down the (0, 1, 0) axis showing the location of the Tl^+ cations in the channels formed by the BiS_6 and PS_4 polyhedra, (C) an individual slab of **IV** as viewed down the (0, 1, 0) axis showing the empty channels for the Tl^+ ions, and (D) coordination environments of Bi1 and Bi2.

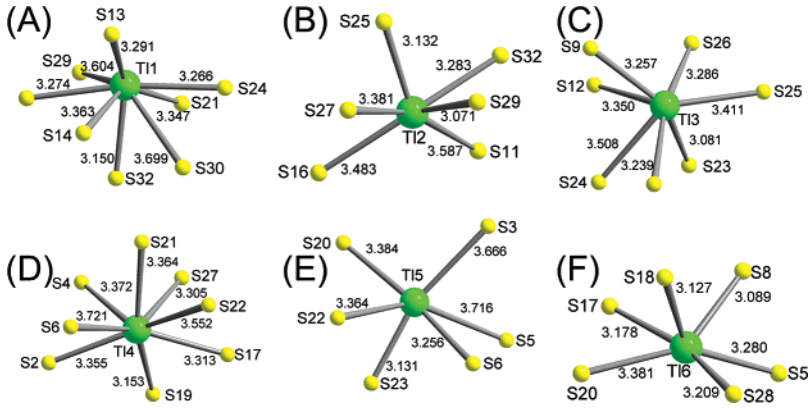

Figure 10. Coordination environments of the crystallographically unique Tl^+ ions in **IV**.

The **IV** slabs consist of trigonal-prismatic and square-pyramidal Bi^{3+} atoms and $[PS_4]^{3-}$ anions (Figure 9C). Each trigonal-prismatic Bi^{3+} atom (Bi1 and Bi2) is surrounded by four $[PS_4]^{3-}$ anions, forming a cross-shaped $Bi(PS_4)_4$ unit. These units are connected with the trigonal-prismatic Bi^{3+} atoms (Bi3, Bi4, Bi5, and Bi6) to form the slab. Bi1 and Bi2 are coordinated by six S atoms to form a distorted trigonal prism (Figure 9D). The geometry is distorted because of the stereochemically active $6s^2$ so-called lone pair of Bi^{3+}. Two $[PS_4]^{3-}$ tetrahedra share one edge with the rectangular planes of the trigonal prism, and the other two $[PS_4]^{3-}$ anions share a corner with the two remaining vertices of the prism. All four $[PS_4]^{3-}$ anions share one edge with the square-pyramidal BiS_5 units Bi3, Bi4, Bi5, and Bi6. The remaining S atoms of the two corner-shared $[PS_4]^{3-}$ units on the pyramid are attached on two BiS_5 units of a different slab.

The Bi−S distances in the trigonal prism vary from 2.709(5) to 2.922(4) Å for Bi1 and from 2.791(5) to 2.883(5) Å for Bi2. The four equatorial bonds in the BiS_5 units range from 2.768(4) to 2.996(5) Å, and the shorter axial distance ranges from 2.627(5) to 2.706(4) Å. The P−S distances in all $[PS_4]^{3-}$ units range from 2.007(6) to 2.064(6) Å.

The coordination number of Tl^+ ions varies from six up to eight S atoms (Figure 10). In particular, Tl1 is surrounded by eight S atoms, forming a distorted dodecahedron with Tl−S distances from 3.159(5) to 3.698(5) Å (Figure 9A). The Tl1 dodecahedron shares a corner through the bridging S29 atom with the six coordinate Tl2 center. The distances in this octahedron vary from 3.071(5) to 3.585(5) Å (Figure 9B). A corner of the distorted $Tl2S_6$ octahedron is shared with the seven-coordinate Tl3, which has Tl−S distances from 3.084(5) to 3.507(5) Å (Figure 9C). Tl4, Tl5, and Tl6 are located in a channel different from that of the other Tl atoms. Tl4 is surrounded by eight S atoms with distances from 3.153(6) to 3.772(6) Å (Figure 9D). Tl5 and Tl6 are six-coordinated with one corner-shared S20 atom and Tl−S

Table 5. Selected Bond Lengths (Å) and Angles (deg) for **IV**, with Standard Uncertainties in Parentheses[a]

Bi1−S31^{i}	2.792(6)	S31^{i}−Bi1−S23	81.2(2)	Tl4−S19	3.153(6)	S14^{ii}−Bi5−S9^{xi}	141.66(16)
Bi1−S23	2.816(6)	S31^{i}−Bi1−S32^{i}	71.59(16)	Tl4−S27^{xv}	3.305(6)	S16−Bi5−S9^{xi}	79.38(17)
Bi1−S32^{i}	2.831(6)	S23−Bi1−S32^{i}	114.29(17)	Tl4−S17^{v}	3.313(6)	S29^{ii}−Bi5−S9^{xi}	114.07(19)
Bi1−S21	2.855(5)	S31^{i}−Bi1−S21	130.47(17)	Tl4−S2^{ix}	3.355(6)	S30^{ii}−Bi5−S10^{xii}	116.23(19)
Bi1−S7^{i}	2.875(5)	S23−Bi1−S21	70.65(15)	Tl4−S21^{xv}	3.363(6)	S14^{ii}−Bi5−S10^{xii}	151.43(16)
Bi1−S10	2.887(5)	S32^{i}−Bi1−S21	83.77(17)	Tl4−S4^{xiii}	3.372(5)	S16−Bi5−S10^{xii}	128.24(14)
Bi1−S11^{i}	3.101(6)	S31^{i}−Bi1−S7^{i}	72.63(15)	Tl4−S22^{xv}	3.551(6)	S29^{ii}−Bi5−S10^{xii}	79.52(15)
Bi2−S27^{i}	2.711(6)	S23−Bi1−S7^{i}	81.47(16)	Tl4−S6^{ix}	3.720(5)	S9^{xi}−Bi5−S10^{xii}	66.91(15)
Bi2−S18	2.776(6)	S32^{i}−Bi1−S7^{i}	137.63(17)	Tl4−S2^{xvii}	3.918(6)	S24^{ii}−Bi4−S11	85.80(16)
Bi2−S26	2.817(5)	S21−Bi1−S7^{i}	137.76(17)	Tl5−S23^{i}	3.130(8)	S24^{ii}−Bi4−S12^{ii}	80.10(16)
Bi2−S17	2.875(5)	S31^{i}−Bi1−S10	147.2(2)	Tl5−S6^{xviii}	3.254(6)	S11−Bi4−S12^{ii}	71.53(14)
Bi2−S15^{i}	2.911(5)	S23−Bi1−S10	131.56(18)	Tl5−S22^{i}	3.363(7)	S24^{ii}−Bi4−S22	73.39(16)
Bi2−S1^{iv}	2.918(5)	S32^{i}−Bi1−S10	91.88(16)	Tl5−S20^{xix}	3.384(6)	S11−Bi4−S22	147.37(17)
Bi3−S19^{viii}	2.703(5)	S21−Bi1−S10	72.84(14)	Tl5−Tl6^{xx}	3.646(2)	S12^{ii}−Bi4−S22	80.18(16)
Bi3−S20^{v}	2.767(5)	S7^{i}−Bi1−S10	106.57(14)	Tl5−S3^{xxi}	3.667(6)	S24^{ii}−Bi4−S13^{ii}	76.10(17)
Bi3−S2	2.845(5)	S31^{i}−Bi1−S11^{i}	80.84(19)	Tl5−S5^{i}	3.717(7)	S11−Bi4−S13^{ii}	81.60(16)
Bi3−S6	2.877(5)	S23−Bi1−S11^{i}	155.09(15)	Tl5−P6^{i}	3.872(6)	S12^{ii}−Bi4−S13^{ii}	145.15(16)
Bi3−S8^{ii}	2.905(5)	S32^{i}−Bi1−S11^{i}	75.83(15)	Tl5−S28^{xxii}	4.072(8)	S22−Bi4−S13^{ii}	116.03(19)
Bi3−S1	3.050(5)	S21−Bi1−S11^{i}	134.22(14)	Tl6−S8^{ii}	3.089(5)	S24^{ii}−Bi4−S8^{ii}	140.93(14)
Bi3−S12^{ii}	3.130(5)	S7^{i}−Bi1−S11^{i}	76.77(15)	Tl6−S18^{vi}	3.128(6)	S11−Bi4−S8^{ii}	112.93(15)
Bi4−S24^{ii}	2.667(5)	S10−Bi1−S11^{i}	67.46(15)	Tl6−S17^{ii}	3.178(6)	S12^{ii}−Bi4−S8^{ii}	74.59(14)
Bi4−S11	2.820(5)	S27^{i}−Bi2−S18	106.13(18)	Tl6−S28^{x}	3.209(6)	S22−Bi4−S8^{ii}	73.33(15)
Bi4−S12^{ii}	2.850(5)	S27^{i}−Bi2−S26	72.87(15)	Tl6−S5^{ii}	3.280(6)	S13^{ii}−Bi4−S8^{ii}	138.07(15)
Bi4−S22	2.894(5)	S18−Bi2−S26	87.6(2)	Tl6−S20^{xxiii}	3.382(5)	S24^{ii}−Bi4−S15	122.32(17)
Bi4−S13^{ii}	2.943(6)	S27^{i}−Bi2−S17	79.90(17)	Tl6−S3^{ii}	3.927(6)	S11−Bi4−S15	127.44(15)
Bi4−S8^{ii}	3.007(5)	S18−Bi2−S17	70.37(16)			S12^{ii}−Bi4−S15	148.21(15)
Bi4−S15	3.104(5)	S26−Bi2−S17	138.48(16)	S1−P1	2.019(7)	S22−Bi4−S15	85.17(16)
Bi5−S30^{ii}	2.687(6)	S27^{i}−Bi2−S15^{i}	103.00(17)	S2−P1	2.033(7)	S13^{ii}−Bi4−S15	66.55(15)
Bi5−S14^{ii}	2.819(5)	S18−Bi2−S15^{i}	124.39(19)	S3−P1^{iv}	2.044(7)	S8^{ii}−Bi4−S15	74.22(14)
Bi5−S16	2.820(5)	S26−Bi2−S15^{i}	146.60(18)	S4−P1^{xi}	2.056(6)	S28^{xiv}−Bi6−S3	95.0(2)
Bi5−S29^{ii}	2.891(6)	S17−Bi2−S15^{i}	69.55(14)	S5−P2	2.024(7)	S28^{xiv}−Bi6−S4^{i}	84.23(19)
Bi5−S9^{xi}	2.921(6)	S27^{i}−Bi2−S1^{iv}	139.15(16)	S6−P2^{ii}	2.044(7)	S3−Bi6−S4^{i}	72.01(15)
Bi5−S10^{xii}	3.035(5)	S18−Bi2−S1^{iv}	87.17(16)	S7−P2^{ii}	2.056(8)	S28^{xiv}−Bi6−S5	75.78(17)
Bi6−S28^{xiv}	2.634(6)	S26−Bi2−S1^{iv}	69.23(14)	S8−P2	2.057(7)	S3−Bi6−S5	79.46(16)
Bi6−S3	2.764(5)	S17−Bi2−S1^{iv}	140.20(16)	S9−P3^{ii}	2.001(7)	S4^{i}−Bi6−S5	143.39(15)
Bi6−S4^{i}	2.829(5)	S15^{i}−Bi2−S1^{iv}	100.24(14)	S10−P3	2.046(8)	S28^{xiv}−Bi6−S25^{i}	70.90(18)
Bi6−S5	2.892(5)	S19^{viii}−Bi3−S20^{v}	73.92(16)	S11−P3^{ii}	2.051(7)	S3−Bi6−S25^{i}	151.65(17)
Bi6−S25^{i}	3.000(6)	S19^{viii}−Bi3−S2	78.81(16)	S12−P3	2.061(7)	S4^{i}−Bi6−S25^{i}	81.94(15)
Bi6−S7^{i}	3.023(5)	S20^{v}−Bi3−S2	111.18(19)	S13−P4	2.020(8)	S5−Bi6−S25^{i}	118.48(16)
Bi6−S14	3.123(6)	S19^{viii}−Bi3−S6	85.91(18)	S14−P4	2.039(7)	S28^{xiv}−Bi6−S7^{i}	113.8(2)
		S20^{v}−Bi3−S6	149.20(17)	S15−P4^{ii}	2.044(8)	S3−Bi6−S7^{i}	128.03(16)
Tl1−S32^{i}	3.150(6)	S2−Bi3−S6	86.68(17)	S16−P4^{ii}	2.065(7)	S4^{i}−Bi6−S7^{i}	148.42(15)
Tl1−S24^{ii}	3.265(6)	S19^{viii}−Bi3−S8^{ii}	76.74(15)	S17−P5^{v}	2.037(7)	S5−Bi6−S7^{i}	68.14(14)
Tl1−S31^{xiii}	3.273(7)	S20^{v}−Bi3−S8^{ii}	82.25(17)	S18−P5^{v}	2.046(7)	S25^{i}−Bi6−S7^{i}	80.28(15)
Tl1−S13^{iii}	3.291(6)	S2−Bi3−S8^{ii}	147.39(15)	S19−P5	2.045(7)	S28^{xiv}−Bi6−S14	136.21(16)
Tl1−S21	3.348(6)	S6−Bi3−S8^{ii}	70.42(14)	S20−P5^{xxv}	2.042(8)	S3−Bi6−S14	116.33(17)
Tl1−S14^{iii}	3.364(6)	S19^{viii}−Bi3−S1	128.11(15)	S21−P6	2.012(7)	S4^{i}−Bi6−S14	78.03(14)
Tl1−S29^{xi}	3.603(6)	S20^{v}−Bi3−S1	82.67(15)	S22−P6	2.016(8)	S5−Bi6−S14	136.57(14)
Tl1−S30^{iii}	3.699(7)	S2−Bi3−S1	67.49(15)	S23−P6	2.047(7)	S25^{i}−Bi6−S14	67.19(14)
Tl2−S29^{iii}	3.071(6)	S6−Bi3−S1	128.03(15)	S24−P6^{i}	2.080(7)	S7^{i}−Bi6−S14	71.08(14)
Tl2−S25^{xiii}	3.132(6)	S8^{ii}−Bi3−S1	145.10(14)	S25−P7	1.998(8)		
Tl2−S32^{i}	3.284(6)	S19^{viii}−Bi3−S12^{ii}	136.28(14)	S26−P7^{xxviii}	2.030(7)		
Tl2−S27^{xv}	3.380(7)	S20^{v}−Bi3−S12^{ii}	72.28(15)	S27−P7^{xxii}	2.059(7)		
Tl2−S16^{xv}	3.482(5)	S2−Bi3−S12^{ii}	139.72(14)	S28−P7^{xxii}	2.074(8)		
Tl2−S11^{i}	3.587(6)	S6−Bi3−S12^{ii}	110.65(16)	S29−P8	2.015(8)		
Tl2−Tl3^{iii}	3.883(2)	S8^{ii}−Bi3−S12^{ii}	71.97(13)	S30−P8	2.042(8)		
Tl2−Tl1^{xv}	4.192(2)	S1−Bi3−S12^{ii}	73.49(13)	S31−P8^{ix}	2.047(7)		
Tl3−S23	3.081(6)	S30^{ii}−Bi5−S14^{ii}	80.53(19)	S32−P8^{ix}	2.061(7)		
Tl3−S30^{iii}	3.239(7)	S30^{ii}−Bi5−S16	89.65(18)				
Tl3−S9	3.257(6)	S14^{ii}−Bi5−S16	71.26(15)				
Tl3−S26^{xvi}	3.287(7)	S30^{ii}−Bi5−S29^{ii}	71.70(16)				
Tl3−S12^{ii}	3.350(5)	S14^{ii}−Bi5−S29^{ii}	84.85(16)				
Tl3−S25^{i}	3.411(5)	S16−Bi5−S29^{ii}	151.97(16)				
Tl3−S24^{ii}	3.508(6)	S30^{ii}−Bi5−S9^{xi}	75.09(18)				

[a] (i) $x, -1.5 - y, 0.5 + z$; (ii) $x, -1.5 - y, -0.5 + z$; (iii) $1 - x, -0.5 + y, 0.5 - z$; (iv) $x, -0.5 - y, 0.5 + z$; (v) $1 - x, -1 - y, 1 - z$; (vi) $2 - x, -1 - y, 1 - z$; (vii) $2 - x, 0.5 + y, 1.5 - z$; (viii) $1 + x, y, z$; (ix) $1 - x, -1 - y, -z$; (x) $2 - x, 0.5 + y, 0.5 - z$; (xi) $x, -1 + y, z$; (xii) $x, -2.5 - y, -0.5 + z$; (xiii) $1 - x, -2 - y, -z$; (xiv) $x, 1 + y, z$; (xv) $1 - x, 0.5 + y, 0.5 - z$; (xvi) $x, -0.5 - y, -0.5 + z$; (xvii) $-1 + x, y, z$; (xviii) $x, y, 1 + z$; (xix) $1 - x, -0.5 + y, 1.5 - z$; (xx) $2 - x, -2 - y, 1 - z$; (xxi) $2 - x, -0.5 + y, 1.5 - z$; (xxii) $x, -2.5 - y, 0.5 + z$; (xxiii) $1 + x, -1.5 - y, -0.5 + z$; (xxiv) $x, y, -1 + z$; (xxv) $-x, -1 - y, 1 - z$; (xxvi) $-1 + x, -1.5 - y, 0.5 + z$; (xxvii) $1 - x, 0.5 + y, 1.5 - z$; (xxviii) $x, 1 + y, 1 + z$; (xxix) $2 - x, -0.5 + y, 0.5 - z$; (xxx) $-1 + x, -1.5 - y, -0.5 + z$; (xxxi) $x, -1 + y, -1 + z$; (xxxii) $2 - x, -2 - y, -z$.

distances in the range of 3.085(4) to 3.717(5) Å (parts E and F of Figure 9, respectively). Selected bond lengths and angles for compound **IV** are given in Table 5.

(d) Compound V. V crystallizes in the monoclinic space group $P2_1/c$ and is isomorphous to $KBiP_2S_7$.[12] The structure is composed of corrugated $[BiP_2S_7]^-$ layers (Figure 11)

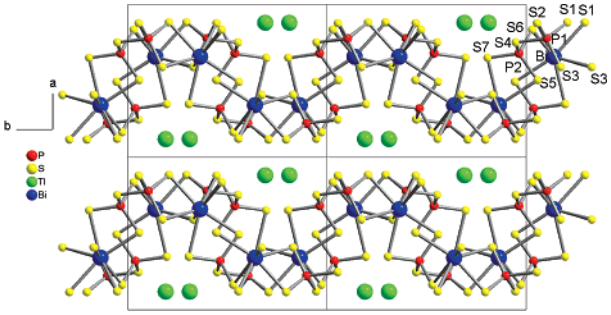

Figure 11. Structure of **V** viewed down the (0, 0, 1) axis showing the corrugated lamellar packing.

separated by eight-coordinate Tl^+ with an average Tl−S distance of 3.34 Å (Figure 12A). Each Bi^{3+} ion is bischelated to three $[P_2S_7]^{4-}$ anions (average Bi−Se bond lengths of 2.92 Å) and chelated by another $[P_2S_7]^{4-}$ anion (Bi−S bond length of 2.778(2) Å; Figure 12B). Table 6 contains selected bond lengths and angles for compound **V**.

(e) Compound VI. This compound is isotypic to $K_3Bi(PS_4)_2$. The structure solution revealed the same straight $[Bi(PS_4)_2]^{3-}$ chains as those in the K analogue (Figure 13A). Furthermore, a comparison of the powder X-ray diffraction patterns with simulated ones from the known K^+-containing phase as well as the solutions discussed here suggested that the compounds were nearly identical. The chains, however, exhibited a position disorder in the Bi^{3+} atoms, which were separated from each other along the chain axis by a distance of approximately 0.85 Å (Figure 13B).

Optical Properties. Diffuse-reflectance measurements suggest that the optical band gaps of the title compounds are smaller than those of the K^+ analogues. The spectrum of **I** indicated that the band gap was about 1.23 eV (Figure 14A), whereas α-$KBiP_2Se_6$ was reported to have a band gap of 1.61 eV.[32] The average Tl−Se distance in the former was 3.38 Å, whereas the average K−Se distance in the latter was 3.36 Å. The similarities in bond lengths are expected given that Tl^+ and K^+ have similar ionic radii (1.5 Å for Tl^+ vs 1.4 Å for K^+).[35] The reduction in the band gap in the Tl^+ analogues is therefore likely because of the increased covalency of the interaction between the metal and Se. In most main-group metal chalcogenides with semiconducting band gaps, the top of the valence band is dominated by chalcogen-based filled p orbitals, whereas the bottom of the conduction band is mainly based on empty p orbitals of the main-group metal.[20] The substitution of K for Tl in K/M/Q structures enhances the Tl−Q bonding through increased covalency, which further broadens the bands near the energy gap, causing it to shrink.[18]

It is not surprising that, given the similarity between the $[BiP_2Se_6]^-$ frameworks in **I** and **II** and the similar Tl−Se bond lengths, the optical band gaps are also similar, showing an absorption edge at 1.27 eV. The band gap of **III** is slightly larger at 1.81 eV, as is expected upon substitution of Se for S in structurally related compounds (i.e., containing a $[P_2Q_6]^{4-}$ anion; Figure 14A).

V was determined to have an optical band gap of 1.87 eV (Figure 14B). The isomorphic analogue of compound **V**, $KBiP_2S_7$, was reported at 2.25 eV.[1e] **IV**, **VI**, and **VII** have optical band gaps of 1.88, 1.98, and 1.97 eV.

Solid-State NMR. Spectra are displayed in Figure 15, and Table 7 presents chemical shifts (CSs), line widths, integrated intensities, chemical shift anisotropies (CSAs), and longitudinal relaxation times (T_1's). The CSs and CSAs of each of the reported thio- and selenophosphate materials are within the ranges expected for related materials.[21,36]

P−Tl *J* Coupling. The spectrum of **V** had two sets of peaks centered at 85.2 and 72.4 ppm with splittings of 481 and 783 Hz, respectively (Figure 15E). One possible cause of these splittings is two-bond P−Tl *J* couplings, and this hypothesis was tested using the isomorphic analogue $KBiP_2S_7$.[1e] The ^{31}P NMR spectrum of the analogue contained two singlet peaks centered at 85.2 and 75.4 ppm (Figure 15H), indicating that the splitting observed in the spectrum of **V** was due to P−Tl coupling. The ^{31}P atoms in the $[P_2S_7]^{3-}$ ion are crystallographically inequivalent, and it is interesting that the P−Tl *J* coupling is observed while the two-bond P−P *J* coupling is not apparent. It was not possible to rationalize the spitting patterns based on numbers of equivalent and inequivalent Tl. ^{203}Tl (30% abundant) and ^{205}Tl (70% abundant) would resonate at 228.89 and 231.14 MHz in a 9.4 T magnet, respectively, and distinct couplings to the different spin $^1/_2$ Tl isotopes were not observed. In liquid-state NMR studies of organophosphorus thallium compounds, distinct $^{31}P-^{203}Tl$ and $^{31}P-^{205}Tl$ couplings were also not observed.

There was additional evidence for two-bond P−Tl *J* coupling in the spectra of other title compounds. The 9.4-T NMR spectrum of **VII** contained two peaks centered at 98.2 ppm with a 490-Hz splitting and three peaks centered at 79.3 ppm with neighboring peak splittings of 1390 and 1180 Hz. At 7 T, the respective splittings were 510, 1390, and 1180 Hz. The constancy of the splitting magnitudes with respect to the magnetic field is a marker of *J* coupling. Similarly, at 9.4 T, the NMR spectrum of **VI** appeared to be a multiplet centered at 79.9 ppm with neighboring peak separations of ∼1400 Hz (Figure 15F). At 7 T, the same splitting magnitudes were observed.

The spectral line widths of the Tl-containing chalcophosphate materials are also relatively broad compared to the chalcophosphate materials that do not contain Tl.[21,36] For example, $KBiP_2S_7$ had a line width of 337 Hz, whereas some of the Tl-containing compounds had line widths greater than 1600 Hz. The increased line widths are likely due, in part, to unresolved P−Tl coupling.

To the best of our knowledge, this is the first example of P−Tl coupling observed in the solid state, although one bond P−Tl coupling in the liquid state has been observed. For example, coupling constants of 3203 and 3144 Hz were

(35) Greenwood, N. N.; Earnshaw, A. *Chemistry of the Elements*; Butterworth Heinemann: Oxford, U.K., 1998; pp 75 and 222.

(36) Regelsky, G. Ph.D. Thesis, University of Münster, Münster, Germany, 2000.

(37) Bryce, D. L.; Wasylishen, R. E. *J. Mol. Struct.* **2002**, *602*−*603*, 463−472.

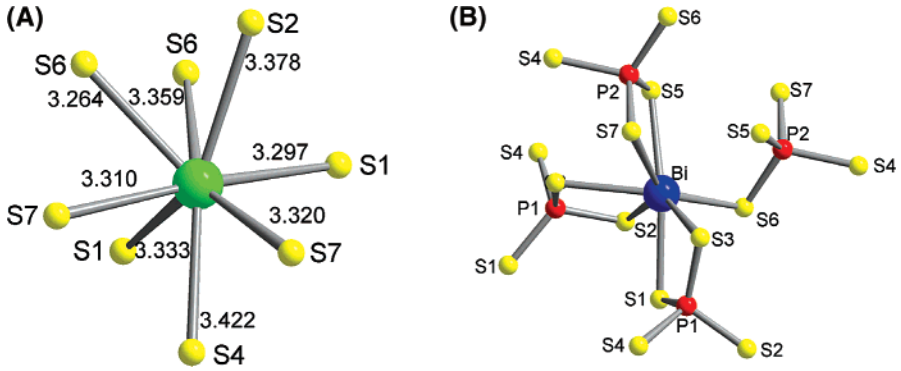

Figure 12. (A) Tl^{+} coordination environment (the Tl atom is green) and (B) coordination environment of Bi^{3+} in V.

Table 6. Selected Bond Lengths (Å) and Angles (deg) for α-**V**, with Standard Uncertainties in Parentheses[a]

Bi−S6	2.7780(18)	S6−Bi−S2	74.63(5)
Bi−S2	2.8238(18)	S6−Bi−S1	82.05(5)
Bi−S1	2.8752(19)	S2−Bi−S1	72.53(5)
Bi−S3^{i}	2.9124(18)	S6−Bi−S3^{i}	144.34(5)
Bi−S5	2.9156(18)	S2−Bi−S3^{i}	70.59(5)
Bi−S3	2.9778(18)	S1−Bi−S3^{i}	94.72(5)
Bi−S7	3.0376(19)	S6−Bi−S5	93.42(5)
		S2−Bi−S5	89.24(5)
Tl−S6^{vi}	3.2640(19)	S1−Bi−S5	161.77(5)
Tl−S1^{vii}	3.2973(18)	S3^{i}−Bi−S5	78.65(5)
Tl−S7^{i}	3.3099(18)	S6−Bi−S3	98.15(5)
Tl−S7	3.3202(19)	S2−Bi−S3	140.53(5)
Tl−S1^{viii}	3.3330(19)	S1−Bi−S3	68.03(5)
Tl−S6^{viii}	3.3589(19)	S3^{i}−Bi−S3	113.61(4)
Tl−S2^{vi}	3.3784(19)	S5−Bi−S3	130.19(5)
Tl−S4	3.4224(18)	S6−Bi−S7	138.27(5)
Tl−S2^{vii}	3.960(2)	S2−Bi−S7	139.31(5)
		S1−Bi−S7	124.82(5)
P1−S1^{ii}	2.019(2)	S3^{i}−Bi−S7	71.41(5)
P1−S3^{ii}	2.022(3)	S5−Bi−S7	69.47(5)
P1−S2^{ix}	2.028(2)	S3−Bi−S7	69.92(5)
P1−S4	2.118(2)		
P2−S7	2.009(2)	S1^{ii}−P1−S3^{ii}	108.31(11)
P2−S5	2.019(3)	S1^{ii}−P1−S2^{ix}	116.52(12)
P2−S6^{xii}	2.037(2)	S3^{ii}−P1−S2^{ix}	109.89(10)
P2−S4	2.118(2)	S1^{ii}−P1−S4	
		S3^{ii}−P1−S4	112.05(11)
		S2^{ix}−P1−S4	98.04(10)
		S7−P2−S5	114.80(11)
		S7−P2−S6^{xii}	110.52(11)
		S5−P2−S6^{xii}	109.84(11)
		S7−P2−S4	100.26(10)
		S5−P2−S4	111.5(1)
		S6^{xii}−P2−S4	109.53(11)

[a] (i) x, 0.5 − y, 0.5 + z; (ii) 1 − x, 0.5 + y, 0.5 − z; (iii) −1 + x, 0.5 − y, −0.5 + z; (iv) −1 + x, y, z; (v) x, 0.5 − y, −0.5 + z; (vi) 1 − x, −0.5 + y, 0.5 − z; (vii) 1 + x, y, z; (viii) 1 + x, 0.5 − y, 0.5 + z; (ix) 1 − x, 1 − y, 1 − z; (x) 2 − x, 1 − y, 1 − z; (xi) 2 − x, 0.5 + y, 0.5 − z; (xii) 1 − x, 1 − y, −z.

detected in spectra of $Ph_2P(Me_2Tl)_2PPh_2$.[38] To our knowledge, our work is also the first example of two-bond P−Tl *J* coupling. Through-space *J* coupling is also possible when there is significant overlap of the van der Waals radii of the coupled nuclei.[37] For the title compounds, there was not a good correlation between the magnitude of *J* and the distance between P and Tl, which suggests that two-bond coupling is dominant. A comparison of these experimental *J* couplings with *J* couplings derived from electronic structure calculations may be one way to now validate the calculation method.

(38) Walther, B.; Bauer, S. *Organomet. Chem.* **1977**, *142*, 177−184.

Splittings due to P−P *J* coupling have been observed in compounds with directly bonded crystallographically inequivalent P atoms.[21] Such splittings were a possibility in compounds **I** and **II**, but they were not observed, likely because of the broad spectral line widths.

Peak Assignments. VII[18] provided an interesting example of a structure with both $[P_2S_6]^{4-}$ and $[PS_4]^{3-}$ anions. The chemical shift ranges of these two anions are known to be overlapped, and differences in the CSA magnitudes for the two anions were used for chemical assignment. The NMR spectrum of **VII** showed two sets of peaks: a doublet centered at 98.2 ppm and a triplet centered at 79.3 ppm (Figure 15G). The crystallographic structure solution contained two inequivalent P sites: one in the $[PS_4]^{3-}$ anion and one in the $[P_2Se_6]^{4-}$ anion. Spinning sidebands were observed only for the doublet, and so the P atom corresponding to this site must have a larger magnitude CSA than the triplet. The magnitude of the CSA of $[PS_4]^{3-}$ has previously been shown to be significantly lower than that of $[P_2S_6]^{4-}$ anions,[21] so the triplet and doublet were therefore assigned to the $[PS_4]^{3-}$ and $[P_2S_6]^{4-}$ units, respectively.

Chemical shift assignment was also made for compounds with crystallographically inequivalent ^{31}P atoms that were in the same type of $[P_xQ_y]^{z-}$ anion. The spectrum of **II** showed three peaks with a ratio of integrated signal intensity of about 1:2:1 with chemical shifts of 48.9, 24.7, and 9.1 ppm (Figure 15B). There were four crystallographically inequivalent P sites with some variation in the numbers of Bi^{3+} and Tl^{+} ions close to the $[P_2Se_6]^{4-}$ anions. These variations were correlated with the chemical shifts using the following scheme. For each P site, spheres of 4-Å diameter were considered around each of the bonded Se atoms, and the total numbers of Bi^{3+} and Tl^{+} ions were counted within these spheres. The 4-Å diameter was a reasonable cutoff for defining proximate metal ions because the Se−metal ion distances formed two groups: one with 2.8 Å < $d_{Se-metal}$ < 4.0 Å and one with $d_{Se-metal}$ > 4.5 Å. Within these spheres, P1 and P3 had three Bi^{3+} and three Tl^{+} ions, P2 had four Bi^{3+} and two Tl^{+} ions, and P4 had two Bi^{3+} and four Tl^{+} ions. The central NMR spectral peak can be attributed to P1 and P3, which have the same number of vicinal Bi^{3+} and Tl^{+} ions, and the other distinct peaks can be attributed to P2 and P4. It is not possible using this method to determine the specific chemical shift that corresponds to each site. This

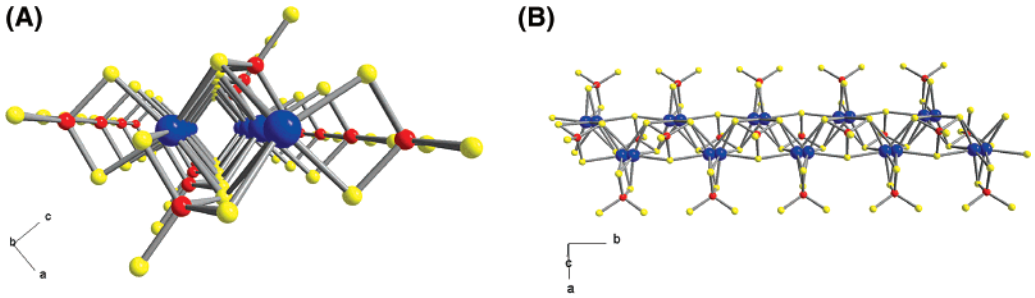

Figure 13. (A) $[Bi(PS_4)_2]^{3-}$ chain that runs down the (0, 1, 0) axis and (B) perpendicular to the (0, 1, 0) axis showing the Bi^{3+} positional disorder. Bi atoms are in blue, and P and S atoms are in red and yellow, respectively.

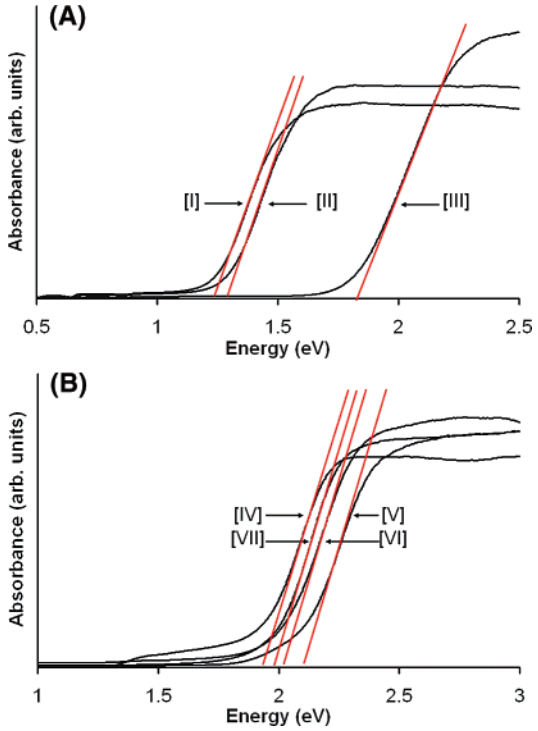

Figure 14. Optical absorption spectra showing energy band gaps of (A) **I** (1.23 eV), **II** (1.27 eV), and **III** (1.81 eV) and (B) **IV** (1.88 eV), **V** (1.87 eV), **VI** (1.87 eV), and **VII** (1.98 eV).

model only groups ^{31}P sites by similarities in coordination and does not predict the magnitude or sign of the chemical shift differences.

Compound **IV** is another example of this approach to assignment. The NMR spectrum showed three peaks with the approximate intensity ratio of 4:1:3 and shifts of 79.3, 75.8, and 71.0 ppm (Figure 15D).[39] There are eight inequivalent P sites, and an assignment was made by grouping them into three distinct coordination environments using a scheme similar to that for compound **II**. However, only proximate Bi^{3+} ions were considered for compound **IV** because the S−Tl distances had a more continuous distribution than that found for compound **II**. The P1-, P3-, and P4-centered $[PS_4]^{3-}$ anions had four proximate Bi^{3+} ions, the P2-centered $[PS_4]^{3-}$ ion had four proximate Bi^{3+} ions, and the four remaining $[PS_4]^{3-}$ anions had two proximate Bi^{3+} ions. It is reasonable that the $[PS_4]^{3-}$ anions with similar coordination

(39) A mathematical deconvolution of the spectrum was only successful when the feature furthest downfield was modeled by two closely spaced peaks.

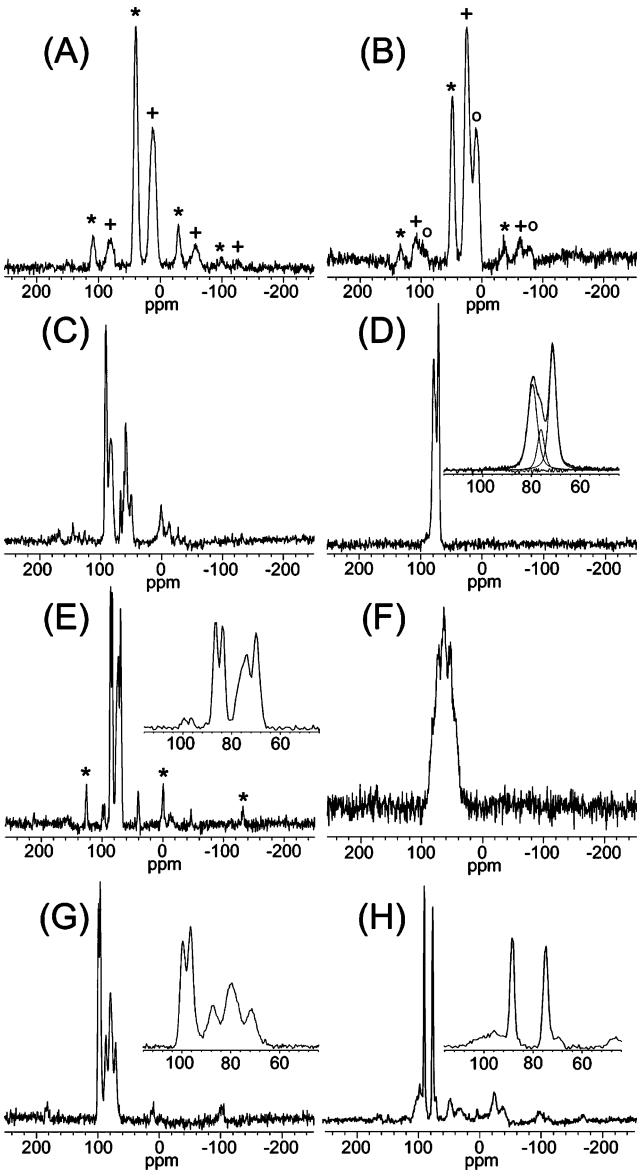

Figure 15. ^{31}P NMR spectra of (A) **I**, (B) **II**, (C) **III**, (D) **IV**, (E) **V**, (F) **VI**, (G) **VII**, and (H) $KBiP_2S_7$. Each spectrum was an average of four scans with a delay between pulses of 5000 s. Each spectrum was processed with ≤100-Hz line broadening. Peaks and their corresponding spinning sidebands are grouped with like symbols. Expanded insets are displayed in (D), (E), (G) and (H) and a deconvolution of the overlapped peaks is also displayed in (D).

environments have the same chemical shifts, and the ratio of the intensities can be explained on this basis.

The numbers of crystallographically inequivalent P atoms and the numbers of distinct shifts were equal for compounds

Table 7. ^{31}P Chemical Shift (CS), Chemical Shift Anisotropy (CSA), and T_1 Values[a]

compd	CS[b] (ppm)	line widths[b] (Hz)	integrated intensities[c]	CSA[d] (ppm)	T_1[e] (s)
I	40.0, 12.4	1060, 1640	100, 90	nd	nd
II	48.9, 24.7, 9.1	1000, 1390, 1650	53, 100, 68	nd	1500 (150)
IV	79.3, 75.8, 71.0	730, 500, 570	100, 30, 91	69	1500 (100)
V	85.2, 75.4	320, 860	67, 100	nd	1750 (150)
VI	79.9	1600	100	nd	1500 (100)
VII	98.2, 79.3	410, 800	91, 100	137, n.o.	1300 (300)

[a] nd = not determined. no = not observable. [b] Uncertainties in CS are approximately ±0.5 ppm, and uncertainties in line widths are approximately ±10 Hz. These parameters were determined by a mathematical deconvolution of the peak with equal contributions from Gaussian and Lorentzian line shapes. [c] Intensities were normalized with the most intense peak set to 100. For compounds with splittings due to *J* coupling, the integrated intensities of the constituent peaks were summed. [d] Principal CSA values were determined using a Herzfeld−Berger analysis computer program (Eichele, K.; Wasylishen, R. E. *HBA 1.5*; Dalhousie University: Halifax, Nova Scotia, Canada, and Universtät Tübingen: Tübingen, Germany, 2006). The reported CSA = $\delta_{11} - \delta_{33}$, i.e., the approximate overall width of the static CS powder pattern. Maximum CSA uncertainties are ±20 ppm. [e] Uncertainties are indicated in parentheses.

I and **V** (parts A and E of Figure 15, respectively). Each peak in the NMR spectrum corresponds to one of these crystallographically inequivalent sites. Chemical shifts were not calculated, and therefore specific peaks cannot at present be attributed to particular crystallographic sites. Impurity peaks and the lack of an accurate crystal structure precluded assignment in compounds **III** and **VI** (parts C and F of Figure 15, respectively).

Concluding Remarks

A broad family of compounds can be stabilized in the Tl/Bi/P/Q (Q = S,Se) system and contains examples of one-, two-, and three-dimensional structural motifs. This high degree of structural diversity likely has its origins in the flexibility of the Bi^{3+} and Tl^{+} coordination environments and also in the flexibility of the Tl−Q interaction with the covalent Bi/P/Q framework. The reaction chemistry of the Tl/Bi/P/S system proved to be more diverse and subtle than we originally expected, and small changes in stoichiometry resulted in different reaction paths and compounds. This explains why we often experience problems with reproducibility with some of the compounds we report here [e.g., **IV** vs **V**]. One reason for this rich chemistry seems to be the ability of the thiophosphate anions to convert from one to another with small changes in the P/S ratio. All three species $[PS_4]^{3-}$, $[P_2S_6]^{4-}$, and $[P_2S_7]^{4-}$, as well as combinations thereof such as in **VII**, were observed.[18]

The corresponding Se system was less diverse, and $[PSe_4]^{3-}$ and $[P_2Se_7]^{4-}$ species were not observed. In selenophosphate chemistry, the most stable species under moderate Lewis basic conditions is the P^{4+} anion $[P_2Se_6]^{4-}$.[10] By slight variation of the stoichiometry of the reaction conditions, it is often possible to produce a given phase in pure form. Because of the increased ionicity, it may also be possible to tune the optical properties of these materials by making solid solutions with K. Such a study is also likely to yield new compounds. Similar richness and diversity might be observed in other Tl/M/P/Q systems perhaps with M = Sb, Au, In, Pd, Zn, Cd, Hg, and the lanthanides.

Solid-state ^{31}P NMR spectroscopy of the reported compounds demonstrates chemical shifts and chemical shift anisotropies similar to those of related materials.[21] It was possible to assign the peaks of inequivalent ^{31}P atoms from the same $[P_xQ_y]^{z-}$ anion type by considering differences in the metal ion coordination to the $[P_xQ_y]^{z-}$ unit and by considering CSA magnitudes. A more specific assignment of peaks would require detailed calculations. Such calculations would be challenging because of the presence of numerous heavy atoms in the structures. Splittings due to P−Tl *J* couplings were observed, and to the best of our knowledge, this is the first example of two-bond P−Tl *J* coupling and the first observation of P−Tl *J* coupling in the solid state.

Acknowledgment. Financial support from the National Science Foundation (Grant DMR-0443783) is gratefully acknowledged. We thank Erin E. Wilson at the University of Michigan for assistance with the setup and data acquisition on the Bruker NMR.

Supporting Information Available: Tables of crystallographic details, atomic coordinates, bond length and angles, anisotropic thermal parameters for all compounds (CIF), and a view of the reciprocal lattice of **VI**. This material is available free of charge via the Internet at http://pubs.acs.org.

IC062465H